npj | parkinson's disease

Article

Published in partnership with the Parkinson's Foundation

https://doi.org/10.1038/s41531-024-00777-0

Calbindin and Girk2/Aldh1a1 define resilient *vs* vulnerable dopaminergic neurons in a primate Parkinson's disease model

Natalia López-González del Rey [1,2,3,4], Nagore Hernández-Pinedo [1,2,10], Megan Carrillo [1,2,5,10], María del Cerro [1,2], Noelia Esteban-García [1,2,3], Inés Trigo-Damas [1,2,5,6], Mariana H. G. Monje [1,2,4,7], José L. Lanciego [5,8], Carmen Cavada [3,9], José A. Obeso [1,2,5] ✉ & Javier Blesa [1,2,5,6] ✉

The differential vulnerability of dopaminergic neurons of the *substantia nigra pars compacta* (SNc) is a critical and unresolved question in Parkinson´s disease. Studies in mice show diverse susceptibility of subpopulations of nigral dopaminergic neurons to various toxic agents. In the primate midbrain, the molecular phenotypes of dopaminergic neurons and their differential vulnerability are poorly characterized. We performed a detailed histological study to determine the anatomical distribution of different molecular phenotypes within identified midbrain neurons and their selective vulnerability in control and MPTP-treated monkeys. In the ventral tier of the SNc (*nigrosome*), neurons rich in Aldh1a1 and Girk2 are intermingled, whereas calbindin is the marker that best identifies the most resilient neurons located in the dorsal tier and ventral tegmental area, recapitulating the well-defined dorsoventral axis of susceptibility to degeneration of dopaminergic neurons. In particular, a loss of Aldh1a1+ neurons in the ventral SNc was observed in parallel to the progressive development of parkinsonism. Aldh1a1+ neurons were the main population of vulnerable dopaminergic nigrostriatal-projecting neurons, while Aldh1a1- neurons giving rise to nigropallidal projections remained relatively preserved. Moreover, bundles of entwined Aldh1a1+ dendrites with long trajectories extending towards the *substantia nigra pars reticulata* emerged from clusters of Aldh1a1+ neurons and colocalized with dense cannabinoid receptor 1 afferent fibers likely representing part of the striatonigral projection that is affected in human disorders, including Parkinson´s disease. In conclusion, vulnerable nigrostriatal-projecting neurons can be identified by using Aldh1a1 and Girk2. Further studies are needed to define the afferent/efferent projection patterns of these most vulnerable neurons.

One of the principal hallmarks of Parkinson's disease is degeneration of dopaminergic neurons in the *substantia nigra pars compacta* (SNc), leading to striatal dopamine deficiency[1]. The onset of Parkinson's disease motor manifestations is typically focal and highly correlated with selective loss of dopaminergic neurons in the SNc and dopamine depletion in the caudal putamen contralateral to the clinically affected body side[2,3]. The greatest loss of dopaminergic neurons is found in the ventral tier of the SNc (vSNc), whereas dopaminergic neurons in the dorsal tier of the SNc (dSNc) and ventral tegmental area (VTA) are less vulnerable[4,5]. More specifically, dopaminergic neurons contained within the so-called *nigrosome* region of vSNc appear to be the earliest and mostly affected[4,6]. Other dopaminergic populations are much less affected or remain intact until the neurodegenerative process is far more advanced many years after diagnosis[4,5,7,8]. This pattern of cell loss is essentially maintained regardless of etiopathogenic disease mechanisms (*i.e.*, genetic, toxin-related, environmental factors, and infectious agents)[9]. This suggests that differential dopaminergic neuronal

A full list of affiliations appears at the end of the paper. ✉e-mail: jobeso.hmcinac@hmhospitales.com; jblesa.hmcinac@hmhospitales.com

vulnerability is primarily related to intrinsic cellular properties and connectivity rather than to specific triggering factors of neurodegeneration[10,11].

Work in rodents has shown significant molecular and genetic heterogeneity among dopaminergic neurons within the midbrain[12,13]. Transcriptomic studies comparing the dopaminergic systems of mice and non-human primates (NHPs) have revealed important inter-species differences[14,15]. Therefore, studies in NHPs are instrumental in ascertaining the onset and key mechanisms underlying the selective vulnerability of midbrain dopaminergic neurons[16]. Recent human and NHPs transcriptomic profiling studies have revealed distinct markers within midbrain neurons that correlate with vulnerability[17–21], however, a precise anatomical correlation is lacking. Moreover, it is unclear whether different dopaminergic subpopulations correspond to the human *nigrosome-matrix* compartmentation[13]. This is particularly relevant, because neuronal vulnerability in the SNc has regional selectivity[10,22,23].

This study addresses molecular vulnerability together with topography selectivity in the SNc of NHPs. We reveal distinct molecularly defined dopaminergic neuron subpopulations in the NHP brain and their differential loss in the MPTP (1-methyl-4-phenyl-1,2,3,6-tetrahydropyridine) parkinsonian model. These subpopulations give rise to dopaminergic projections that, despite some overlap, target distinctively specific basal ganglia regions (*i.e.* putamen and globus pallidus) and show a differential degree of susceptibility to MPTP.

Results

Nigrostriatal damage following MPTP-treatment

The density of nigrostriatal terminals in control and MPTP-treated NHPs was first assessed by measuring the optical density within tyrosine hydroxylase (TH) stained coronal sections. A progressive reduction in TH immunoreactivity with increasing motor impairment was observed in the striatum of all MPTP-treated monkeys as previously reported in the same model (Supplementary Fig. 1a–c)[24,25]. Regarding intra-striatal changes, the pre-commissural putamen was relatively less affected than the post-commissural putamen and caudate nuclei (Supplementary Fig. 1d, e). There was also a clear immunoreactivity gradient in the dorsoventral axis, which was already apparent in the asymptomatic group. The *nucleus accumbens* showed the best preservation of TH immunoreactivity (Supplementary Fig. 1a). To elucidate the anatomical location and specific molecular markers underlying differential vulnerability of dopaminergic cellular phenotypes, double immunofluorescence for different pairs of antibodies was performed throughout the rostrocaudal axis of the NHP midbrain.

Patterns of calbindin expression in the ventral midbrain

Intense calbindin (Cb) neuropil staining was observed in the *substantia nigra pars reticulata* (SNr), together with minimal Cb staining in several patchy areas through the vSNc and the VTA (Fig. 1, Supplementary Fig. 2). These areas with minimal Cb staining formed a complex three-dimensional continuum and comprised densely-packed TH+ neurons, matching the so-called *nigrosome* region in the human midbrain[26] (Fig. 1a). This region corresponds to the vSNc tier, and it is related to the densocellular region and the cell columns described by other authors[27–31]. The region enriched in Cb+ neuropil and Cb+ neurons is termed *matrix* in keeping with an analogous description reported for the human midbrain[26], and includes the dSNc, part of the dorsal VTA and the SNr.

In control monkeys, double immunofluorescence for TH+ and Cb+ revealed that 74% of TH+ neurons were located within the Cb- region defined as the *nigrosome*, whereas the remaining 26% of TH+ neurons were found within the *matrix* compartment (Fig. 1b). On average, colocalization of TH and Cb was observed in 14% of neurons; these dopaminergic cells were located in the dSNc and VTA (Fig. 1c). TH+ neurons located in the *nigrosome* lacked Cb immunoreactivity.

A non-homogeneous reduction in the number of TH+ neurons was observed after MPTP intoxication. Neuronal loss was higher in the *nigrosome* (54%) than in the *matrix* (41%) (Fig. 1d). Cell loss in the *nigrosome* (vSNc) was progressive and parallel to the degree of parkinsonism of MPTP-treated monkeys (Fig. 1e). In other words, monkeys with the greatest loss of TH+ neurons in the *nigrosome* (77%) were those that showed the most severe parkinsonism. In contrast, dopaminergic cell loss was roughly similar within the *matrix* compartment across all MPTP-treated groups (47% in the parkinsonian group) (Fig. 1e).

In MPTP-treated monkeys, dopaminergic neurons positive for Cb (TH + /Cb +) were more resistant to MPTP treatment (15% of cell loss) than neurons lacking Cb (TH + /Cb-) (55% average cell loss). In the parkinsonian group, percentages of dopaminergic cell loss were 22% and 76%, respectively, for TH + /Cb+ and TH + /Cb− (Fig. 1f-g).

Patterns of Girk2 expression in the ventral midbrain

Double immunofluorescence for TH and G-protein-activated inward rectifying potassium type 2 (Girk2) revealed marked preferential expression of Girk2 in dopaminergic neurons of the vSNc (Fig. 2a), with variation in the intensity of staining (Fig. 2c). Girk2 expression followed a dorsoventral and mediolateral gradient, with neurons within the dSNc and VTA showing very low Girk2 expression (Fig. 2a; Supplementary Fig. 3). Girk2 staining was present in 85% of all midbrain TH+ neurons, with the remaining TH+ neurons (15%) displaying none or weak Girk2 immunoreactivity, the latter confined to the dSNc and VTA (Fig. 2d). Double immunofluorescence for Cb and Girk2 revealed that most of the neurons that showed the highest expression levels of Girk2+ were in the *nigrosome* compartment and lacked Cb expression (84%; Fig. 2b and Fig. 2e; Supplementary Fig. 4). Moreover, the percentage of double-labeled neurons with Girk2 and Cb was very low (5%; Fig. 2e). Girk2 expression was not restricted to dopaminergic cell somata; it was also observed in the dendritic trees of TH+ neurons located in the vSNc (Fig. 2a; Supplementary Fig. 3). Some Girk2+ fibers in the ventral SNr did not colocalize with TH (Fig. 2a; Supplementary Fig. 3). None or very faint Girk2 expression was found in other catecholaminergic nuclei of the brain (Supplementary Fig. 5). In terms of vulnerability, the Girk2+ population matches the Cb- population and is highly vulnerable to MPTP. This observation, together with the uneven intensity of Girk2 neuronal staining, led us to omit TH + /Girk2+ vs TH + /Girk2- neuronal quantification as part of the analysis. Instead, we focused on the Aldehyde Dehydrogenase 1 Family Member A1 (Aldh1a1) population.

Patterns of Aldh1a1 expression in the ventral midbrain

In the ventral midbrain of control monkeys, neurons which expressed Aldh1a1 were distributed within specific clusters (Figs. 3 and 4; Supplementary Fig. 6). Neurons co-expressing TH and Aldh1a1 (TH + / Aldh1a1 +) comprised up to 71% of the total number of midbrain dopaminergic neurons, showing a sharp preference for location within the vSNc and the VTA (Fig. 4c). Catecholaminergic cell groups outside the midbrain dopaminergic neurons, including the olfactory bulb and *locus coeruleus*, did not show Aldh1a1 expression (Supplementary Fig. 7). Double immunofluorescence for Aldh1a1 and Cb revealed that virtually all Aldh1a1+ neurons are negative for Cb (97%) and indeed are preferentially located within the *nigrosome* compartment (Fig. 4a, d; Supplementary Fig. 8). Double immunofluorescence for Girk2 and Aldh1a1 showed up to three different neuronal phenotypes (Fig. 4b, e; Supplementary Fig. 9): (i) Aldh1a1 + /Girk2+ neurons, representing the most abundant phenotype (72%); (ii) Aldh1a1-/Girk2+ neurons, 15% of the total number of neurons and preferentially located in lateral territories of the SNc; and (iii) Aldh1a1 + /Girk2- neurons (none or weak Girk2 staining), being 13% of the total number of neurons, with an exclusive location in the VTA (Supplementary Fig. 9).

Aldh1a1+ staining was strikingly evident in dendritic processes with long trajectories arising from specific clusters of neurons: these dendrites extend dorsoventrally in the SNr (Fig. 5a, b). This was most evident in rostral sections (Supplementary Fig. 6). These long dendritic processes were also Girk2+ (Fig. 5c) and had a clear trend to be grouped into thick bundles that overlapped with dense cannabinoid receptor type 1 (CBR1) expressing fibers extending dorsally within the SNr, likely representing so-called *dendron bouquets*[32] (Fig. 5d; Supplementary Fig. 10c). CBR1-immunoreactive

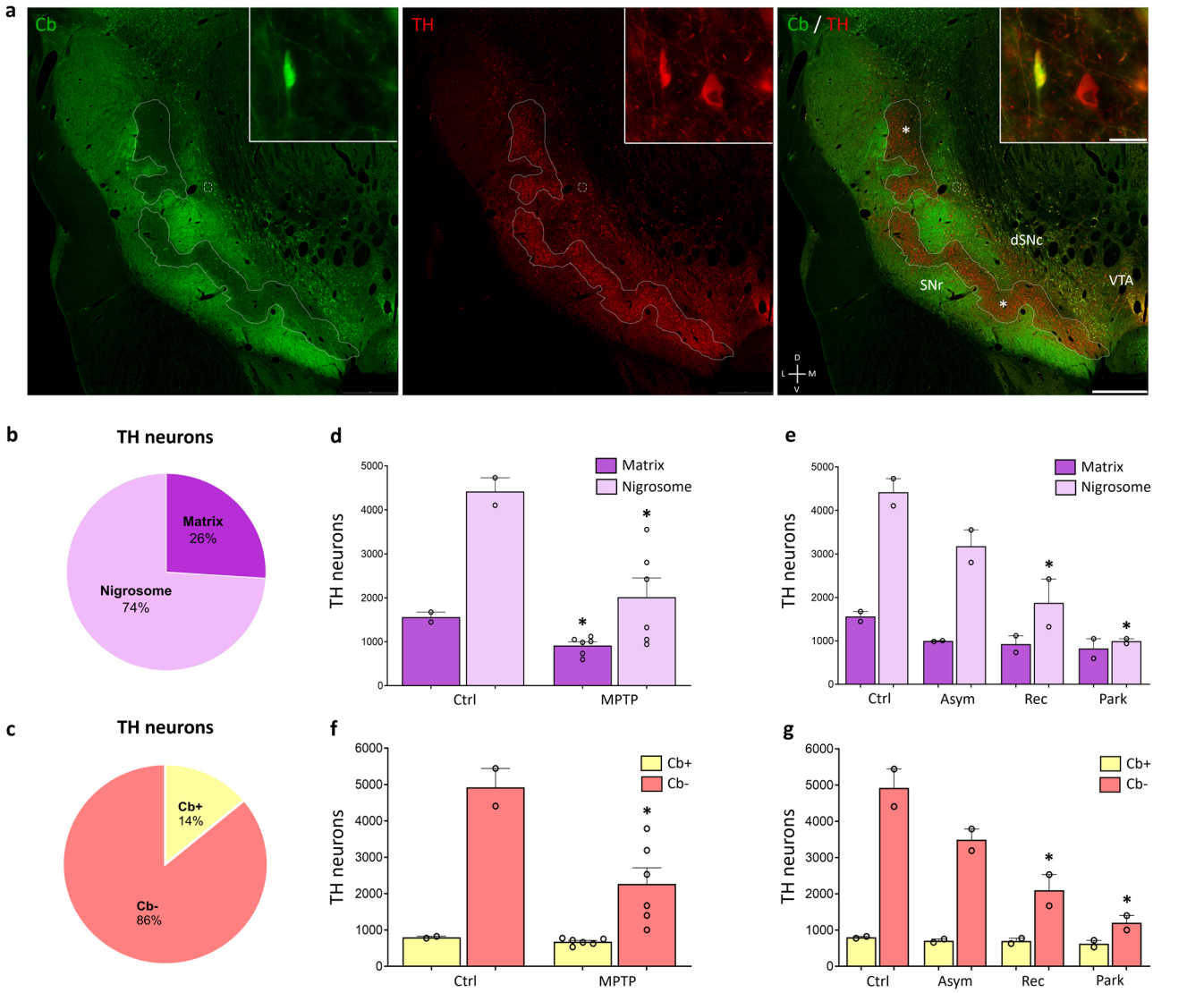

Fig. 1 | Pattern of calbindin expression in the ventral midbrain. a Representative images of TH and Cb immunohistochemistry in the midbrain of control monkeys. Dashed insets at higher magnification of TH+ and Cb+ cells. **b** Percentage of TH+ neurons constraint within *nigrosome* and *matrix* in the control monkey's midbrain ($n = 2$; 5978 ± 281 neurons). **c** Percentage of TH+ neurons co-expressing Cb in the control monkey's midbrain ($n = 2$; 5724 ± 359). **d**, **e** Loss of TH+ neurons in the *matrix* and *nigrosome* compartments in control and MPTP-treated monkeys ($n = 2$/group; MPTP $n = 6$). **f**, **g** Loss of TH + /Cb+ and TH + /Cb- neurons in the control and MPTP-treated monkeys ($n = 2$/group; MPTP $n = 6$). Data represent mean + SEM. Symbols indicate significant differences compared with control $^*P < 0.05$. Ctrl, control; Asym, asymptomatic; Rec, recovered; Park, parkinsonian; * symbol indicate *nigrosome* calbindin-poor region; dSNc: Dorsal *Substantia nigra pars compacta*; SNr: *Substantia nigra pars reticulata*; VTA: Ventral Tegmental Area; D: dorsal; V: ventral; M: medial; L: lateral. Scale bar: 1 mm (inset 50 µm).

bundles climbed along Aldh1a1+ dendrites and neurons (Fig. 5d; Supplementary Fig. 10c). Within the SNr, the CBR1 immunoreactive bundles did not overlap with Cb neuropil immunoreactivity (Fig. 5e; Supplementary Fig. 10d).

To evaluate to what extent Aldh1a1 expression may be linked to dopaminergic cell vulnerability, the numbers of TH + /Aldh1a1+ and TH + /Aldh1a1- neurons were quantified in MPTP-treated macaques (Fig. 4f, g). An evident massive loss of TH + /Aldh1a1+ neurons was observed. This phenotype was significantly more susceptible to degeneration than TH + /Aldh1a1- neurons (Fig. 4h). A gradual TH + /Aldh1a1+ neuronal loss occurred in parallel to the development of parkinsonism, whereas no major differences were found in terms of TH + /Aldh1a1- cell loss across the different MPTP-treated groups (Fig. 4i). Interestingly, the parkinsonian motor phenotype was observed when the TH + /Aldh1a1+ neuronal cell loss was more than 60%. Moreover, in these monkeys there was a clear difference between the TH + /Aldh1a1+ (60%) *vs* TH + /Aldh1a1- (40%) cell loss (Fig. 4j). Remarkably, monkeys that exhibited net and stable parkinsonism showed almost complete loss of TH neurons and processes (Fig. 6).

Aldh1a1+ neurons define the nigrostriatal dopaminergic projection

Two injections into the caudate, three injections into the putamen, and two injections in the globus pallidus were selected for analysis after confirming the accurate placement of the tracers (Supplementary Fig. 11a–e). Neurons containing the tracer injected in the caudate and putamen were particularly abundant in the vSNc while neurons containing the tracer delivered in the globus pallidus appeared rather uniformly scattered in the SNc and VTA.

Among the neurons innervating the caudate nucleus and the putamen, 65% and 88% of cholera toxin subunit B (CTB) labeled neurons were Aldh1a1 +, respectively (Fig. 7a, b). By contrast, only a minority of nigropallidal-projecting neurons express Aldh1a1 (21% for the external division of the pallidus (GPe) and 3% for the internal division of the globus pallidus (GPi)) (Fig. 7c, d, g). To further determine if this distinct origin was

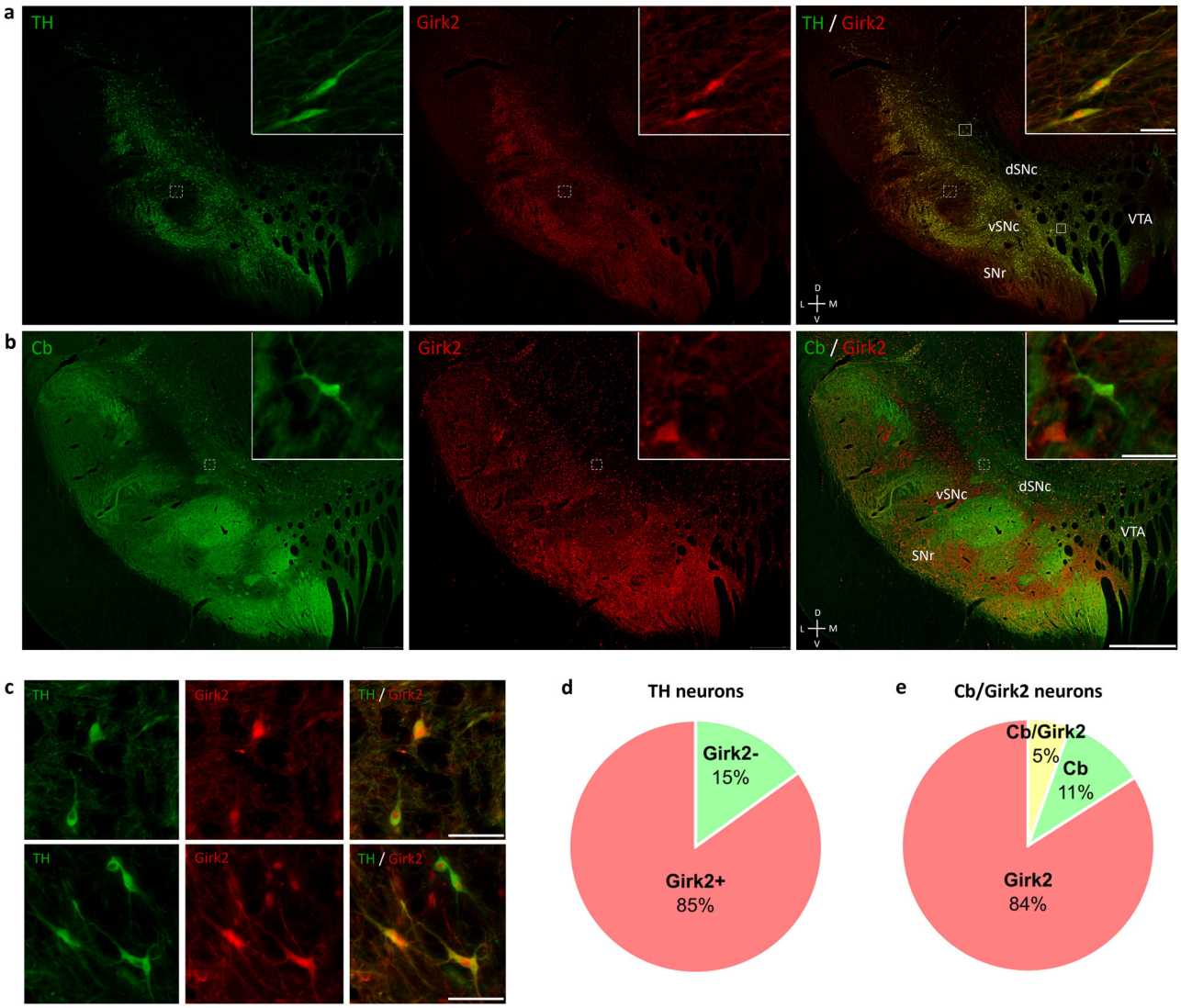

Fig. 2 | Pattern of Girk2 expression in the ventral midbrain. a Representative images of TH and Girk2 immunohistochemistry in the midbrain of control monkeys. Dashed insets at higher magnification of TH+ and Girk2+ cells. Solid inset in **c**. **b** Representative images of Cb and Girk2 immunohistochemistry in the midbrain of control monkeys. Dashed insets at higher magnification of Cb + /Girk2+ cells. **c** Magnified images of solid insets in **a** showing representative TH + /Girk2+ cells with varying intensities of Girk2 staining (i.e., weakly double-stained neurons). **d** Percentages of expression of TH + /Girk2+ in the control monkey midbrain ($n = 2$; 3809 ± 645 neurons). **e** Percentages of co-expression of Cb + /Girk2+ in the control monkey midbrain ($n = 2$; 2914 ± 304 neurons). dSNc Dorsal *Substantia nigra pars compacta*, vSNc: Ventral *Substantia nigra pars compacta*; SNr: *Substantia nigra pars reticulata*; VTA: Ventral Tegmental Area; D: dorsal; V: ventral; M: medial; L lateral. Scale bar: 1 mm (inset **a**: 100 µm; inset **b**: 50 µm).

associated with differential vulnerability, we compared the dopaminergic innervation of the striatum and the GPe and GPi in the same MPTP-treated monkeys. Dopaminergic projection was more profuse in the GPi than in the GPe in control animals. Although a marked reduction on TH+ terminals was observed in caudate and putamen nuclei (up to 87% of loss of dopaminergic terminals in the parkinsonian group) (Supplementary Fig. 1), both the length and density of TH+ axons remained unchanged at the level of the GPe or GPi nuclei (Fig. 7e, f, h, i).

Discussion

In this study, we have identified dopaminergic neuron subtypes in the SNc of the NHP brain and defined their distinct anatomical distribution, projection patterns, and differential vulnerability to MPTP toxicity. We demonstrate that Aldh1a1+ and Girk2+ neurons are highly enriched and intermingled in the vSNc, where cellular vulnerability is highest, in contrast with the more resilient dorsal neurons that express Cb. Aldh1a1+ neurons are the main source of the vulnerable dopaminergic nigrostriatal projection and receive CBR1 afferents. The loss of Aldh1a1+ neurons in the vSNc territory is in keeping with the onset of parkinsonism in our MPTP monkey model. Bearing in mind that Aldh1a1+ neurons were characterized as the dopaminergic cell phenotype predominantly affected in Parkinson´s disease patients, these findings support and expand the evidence of subtype-specific vulnerabilities underlying the pathophysiology of Parkinson´s disease.

Following progressive MPTP-driven toxicity, dopaminergic neuronal loss was consistently greater in the vSNc-*nigrosome* region than in the dorsomedial *matrix* region as described in Parkinson´s disease patients[4]. Of note, the Aldh1a1 + /Girk2+ and Cb+ subpopulations match fairly well with the *nigrosome-matrix* concept, respectively, in terms of anatomic localization and vulnerability[13]. They also align with the SOX6-Cb axis recently reported in humans[17], macaques[18] and mice[33]. Our findings confirm the relative sparing of dopaminergic neurons that express Cb in the SNc and the VTA[34–38], while Aldh1a1 and Girk2 best correlate with the distribution of

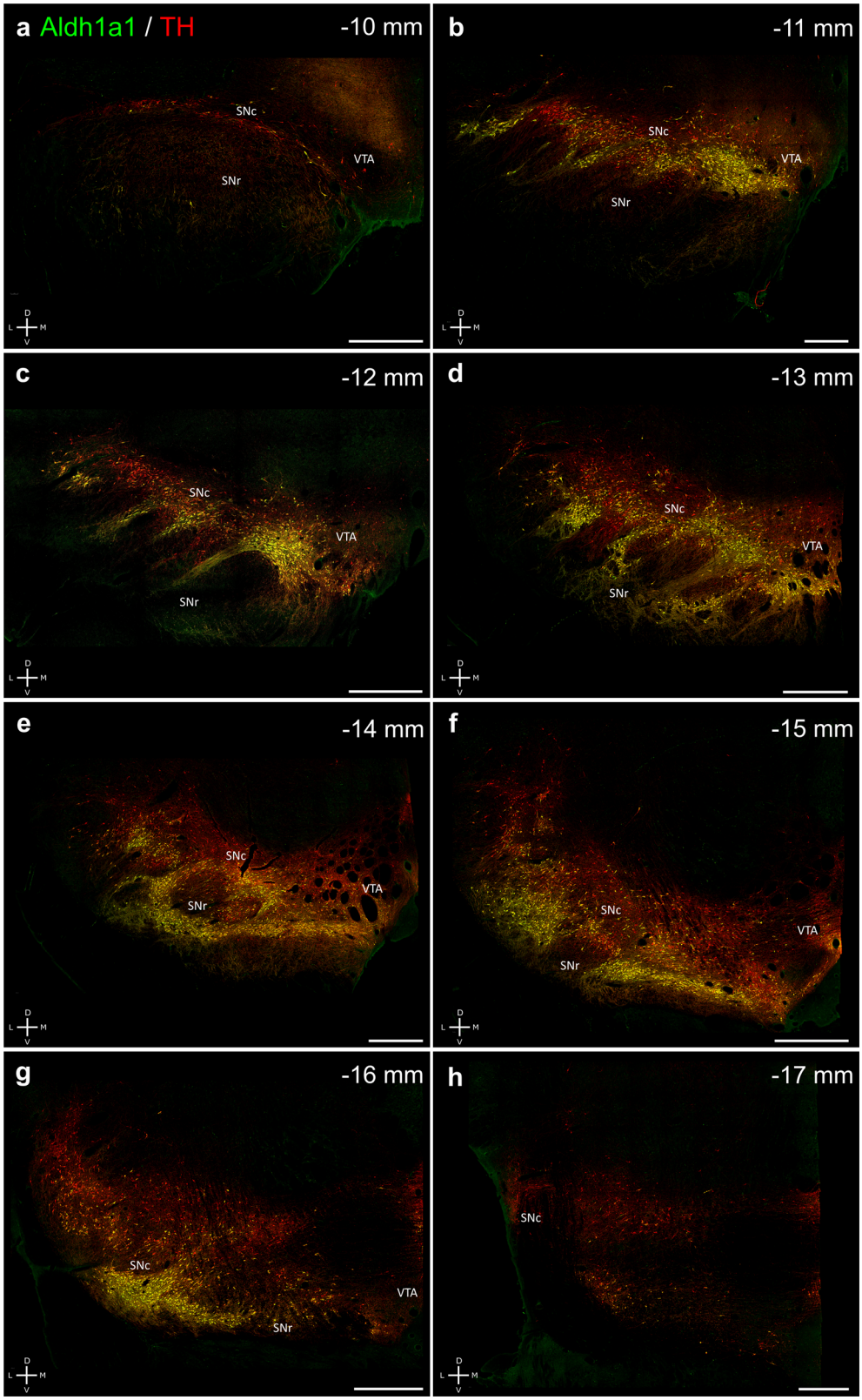

Fig. 3 | Pattern of Aldh1a1 expression in the ventral midbrain. a–h Representative images of coronal sections immunostained for TH and Aldh1a1 from rostral (bregma -10 mm) to caudal (bregma -17 mm) (left to right, top to bottom). Note how the localization of Aldh1a1+ neurons is restricted to the ventral part of the SNc in the control monkey midbrain. Numbers in upper-right corners indicate millimeter distances from bregma from the atlas of Paxinos et al. [105]. SNc: *Substantia nigra pars compacta*; SNr: *Substantia nigra pars reticulata*; VTA: Ventral Tegmental Area; D: dorsal; V: ventral; M: medial; L: lateral. Scale bar: 1 mm.

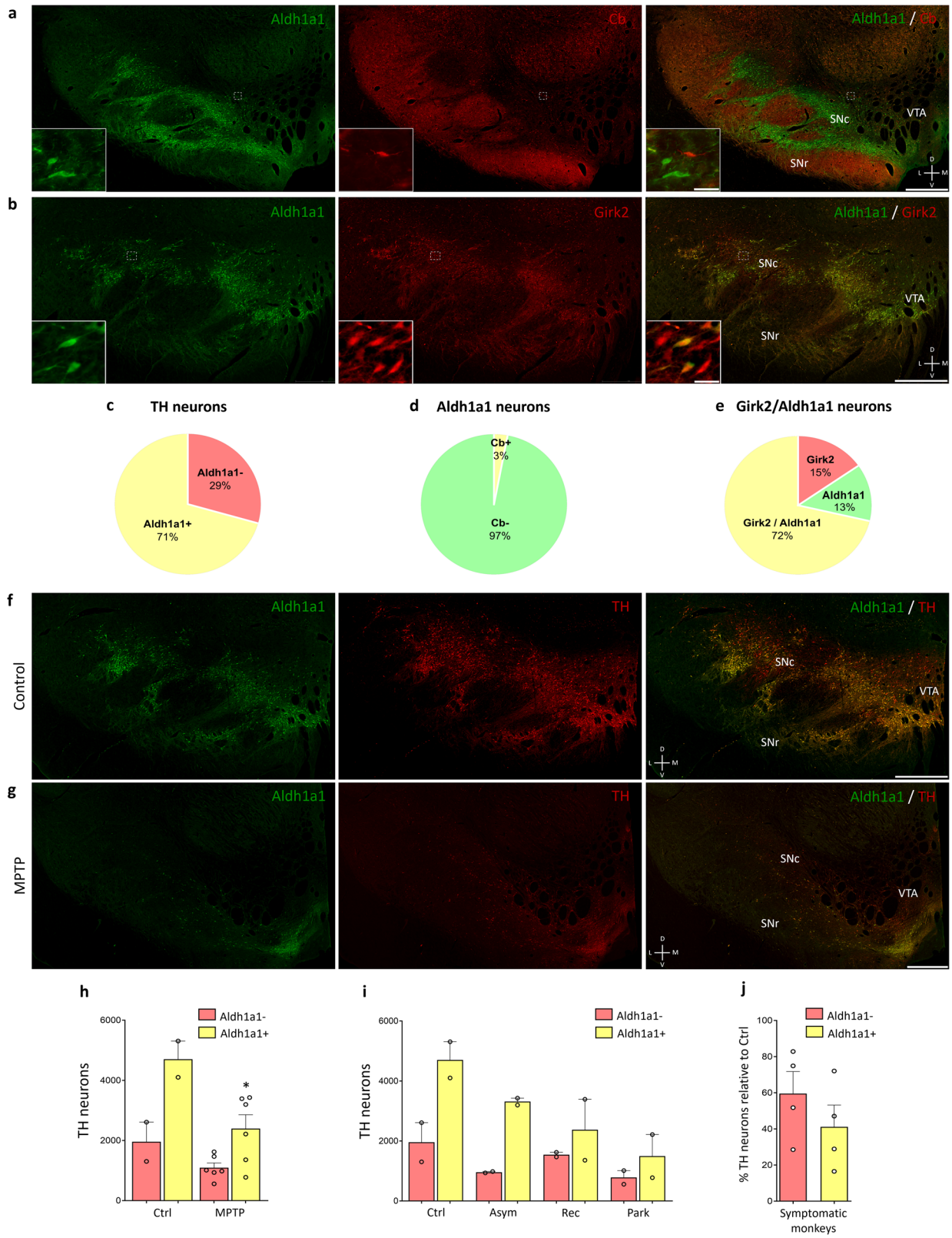

vulnerable neurons[33,39–42]. Several studies in rodents and humans have reported that Girk2 and Cb are not co-expressed in dopaminergic neurons and that expression of Girk2 can discriminate between vulnerable and resilient dopaminergic neurons in the vSNc and the dSNc respectively[43–47]. However, comparable information in monkeys is still very limited[18,48]. Our results indicate that Cb and Girk2 are expressed in different subpopulations and that vulnerable dopaminergic neurons within the vSNc express high levels of Girk2. Moreover, Girk2 expression follows a clear dorsoventral and mediolateral gradient, with the dSNc and VTA containing less Girk2 as described in mice and humans[43,44,49].

Aldh1a1+ neurons appear to be a subpopulation of Girk2+ neurons that form marked clusters which are highly vulnerable to MPTP toxicity,

Fig. 4 | Pattern of Aldh1a1 expression in the ventral midbrain and vulnerability. **a** Representative images of Aldh1a1 and Cb immunohistochemistry in the midbrain of control monkeys. Dashed insets at higher magnification of Aldh1a1+ and Cb+ cells. **b** Representative images of Aldh1a1 and Girk2 immunohistochemistry in the midbrain of control monkeys. Insets at higher magnification of Aldh1a1+ and Girk2+ cells. **c** Percentages of expression of TH + /Aldh1a1+ in the control monkey midbrains ($n = 2$; 6661 ± 776 neurons). **d** Percentages of expression of Aldh1a1 + / Cb+ in the control monkey midbrains ($n = 2$; 2736 ± 365 neurons). **e** Percentages of expression of Aldh1a1 + /Girk2+ in the control monkey midbrains ($n = 2$; 3182 ± 459 neurons). **f**, **g** Representative images of double immunohistochemically labeled neurons for Aldh1a1 and TH in the midbrain of a control **f** and a parkinsonian **g** monkey at the level of the third cranial nerve. **h**, **i** Quantification of TH + / Aldh1a1+ and TH + /Alh1a1- neurons in control and MPTP-treated monkeys ($n = 2$/group; MPTP $n = 6$). **j** Percentages of TH + /Aldh1a1+ and TH + /Aldh1a1- neurons in symptomatic monkeys (Rec+Park; $n = 4$) with respect to the control group ($n = 2$). Data represent mean + SEM. Symbols indicate significant differences compared with control $^*p < 0.05$. Ctrl, control; Asym, asymptomatic; Rec, recovered; Park, parkinsonian. SNc: *Substantia nigra pars compacta*; SNr: *Substantia nigra pars reticulata*; VTA: Ventral Tegmental Area; D: dorsal; V: ventral; M: medial; L: lateral. Scale bar: 1 mm (inset 50 μm).

highlighting a high inter-species analogy and specificity[40,42]. Interestingly, the group of Aldh1a1+ neurons located in the VTA expressed very low or no levels of Girk2. This subpopulation of VTA Aldh1a1 neurons is not especially vulnerable in Parkinson´s disease patients[39], MPTP-treated mice[41], or seemingly in our MPTP monkey model (Fig. 4g), suggesting that the sole expression of Aldh1a1 is not the cause of vSNc vulnerability. Indeed, Aldh1a1+ neurons in mice can be further divided into different subpopulations with additional functional heterogeneity[50,51]. Actually, a specific subpopulation of Aldh1a1+ neurons in the SNc that express angiotensin II receptor type 1_(AGTR1) is highly susceptible to neurodegeneration in Parkinson´s disease patients[17].

Our data support and expand some phenotypic features that define highly vulnerable SNc neurons. Thus, those that are Cb-/Girk2 + / Aldh1a1+ exhibit the highest vulnerability. Several other cellular markers of vulnerability have been described in the midbrain[11,13]. To what extent these factors play a pathogenic role in the origin and mechanisms of neurodegeneration or are mere bystanders is not defined. Certainly, Girk2 and Aldh1a1 play an important role in functions that are altered in Parkinson´s disease patients such as calcium homeostasis, cholesterol modulation, and dopamine metabolism[52–55]. These neurons (but not those that are Cb +) present autonomous pacemaking activity based on L-type voltage-dependent Ca2+ channels and show auto-receptor dependent regulation of dopamine release[56,57]. Importantly, Aldh1a1 is not expressed in any other catecholaminergic group[42,58,59], and other catecholaminergic neurons do not express Girk2 or only exhibit low levels. Thus, Girk2+/Aldh1a1+ neurons identify a unique dopaminergic subtype within the vSNc that are especially relevant in Parkinson´s disease. However, it is noteworthy that NHPs (or any other animal) do not develop a Parkinson´s disease-like neurodegeneration spontaneously. Accordingly, these vulnerability factors as well as other putative mechanisms may be necessary but not sufficient for nigrostriatal degeneration.

Our data show that a large proportion of the highly vulnerable nigroputaminal projection neurons express Aldh1a1 (88%). On the other hand, the majority of nigropallidal dopaminergic neurons were Aldh1a1- and were relatively spared. The small proportion of Aldh1a1 neurons projecting to the pallidum could correspond to the nigrostriatal collaterals that arborize in the pallidum and subthalamic nucleus[60,61]. This is consistent with previous studies that have suggested nigrostriatal and nigroextrastriatal projections arise from different groups of midbrain dopaminergic neurons[31,36,62–64] and show differential vulnerability, with the nigropallidal projection being much less affected[62,64,65]. In mice, Aldh1a1+ and Girk2+ neurons project principally and massively to the dorsolateral striatum, while Cb+ projections are biased toward more ventromedial striatal regions and extra-striatal regions[42,45,47,66,67]. The differential susceptibility to neurodegeneration of striatal and extra-striatal projections suggests that the projection pattern of diverse populations of dopaminergic neurons can be a relevant factor determining their vulnerability[11,67,68]. Likewise, different Aldh1a1+ subpopulations may have topographically different projections through the striatum, linking together vulnerable regions of the nigrostriatal system, both at origin and at destination[42,66,67]. Interestingly, Aldh1a1 is responsible for degradation of DOPAL, which triggers alpha-synuclein mediated neurotoxicity at the synaptic level, leading to neurodegeneration[69]. In the near future, further studies defining subpopulations of Aldh1a1+ and Girk2+ dopaminergic neurons and their connectivity will probably unravel further microcircuits more specifically linked to the most vulnerable SNc neurons. This in turn could facilitate the development of specific neurorestorative/protective therapies.

We have shown here that Girk2 is abundant in dopaminergic processes in monkeys, and more importantly, that the bundles of long dendrites that extend ventrally into the SNr region emerge specifically from clusters of Aldh1a1+ neurons and coincide with dense CBR1-expressing fibers that closely resemble the so-called *dendron-bouquets* in mice[32,70–72]. Interestingly, stable parkinsonism in our monkeys was paralleled with an almost complete loss of ventral neurons and dendrites. This concurs with recent data in mouse models which showed how overt parkinsonian features appeared not only in association with striatal dopamine depletion but with the onset of somatodendritic SNc dopamine release impairment[73–75]. Indeed, extensive Aldh1a1+ neuron loss coincided with the onset of motor manifestations in our MPTP monkey model, in keeping with their selective motor related activity[42,51]. We speculate that loss of Aldh1a1 neurons may lead to presynaptic dysregulation of nuclei that compensate and define basal ganglia neuronal output[76–80]. This could also involve a role for CBR1s in modulating the function of these clusters of Aldh1a1+ dopaminergic neurons[70,78,81,82]. Of relevance, CBR1 in the SNr is confined to striatonigral and subthalamonigral terminals[83–85] and the major source of excitatory input to Aldh1a1+ neurons comes from the subthalamic nucleus[42]. Additionally, the vast gabaergic, glutamatergic, and cholinergic inputs to these neurons[32,86,87] could make them more vulnerable or prone to energy failure[88,89].

In sum, the available data indicate that Aldh1a1+ neurons may play a critically relevant function in dopamine release in both the substantia nigra and the striatum and, accordingly, in the regulation of motor functions and motivated behavior[90,91]. Moreover, the refined mechanisms that regulate vSNc neuron activity intuitively suggest a tight, possibly causal, relationship with their exquisite vulnerability for neurodegeneration in Parkinson´s disease.

The relatively low number of animals used here may be viewed as a potential limitation. However, the results were consistently comparable across monkey groups, showing minimal group variations in identified neuronal subpopulations, distribution, and intracellular location. Also, we had to optimize the study to minimize the number of monkeys used (e.g., opting for the lowest possible count and only males) due to the current worldwide shortage[92] and the general trend to reduce experiments involving NHPs.

Unfortunately, we failed to generate reproducible and consistent immunohistochemical staining for other cellular markers of vulnerability with proven performance in rodents. This is open to further testing in the future. It would have been desirable to further define molecularly different subpopulations of Aldh1a1+ and Girk2+ dopaminergic neurons for more in-depth circuit studies[51,90]. Similarly, smaller tracer injections targeting more specific rostral, medial, and caudal territories of the caudate and putamen will be needed.

In conclusion, we have validated and expanded to the primate brain previous findings in Parkinson´s disease rodent models by describing in detail that Girk2 and Aldh1a1 are crucial markers sustaining cell-specific vulnerability of dopaminergic neurons. Additional efforts are required to establish detailed projection patterns for

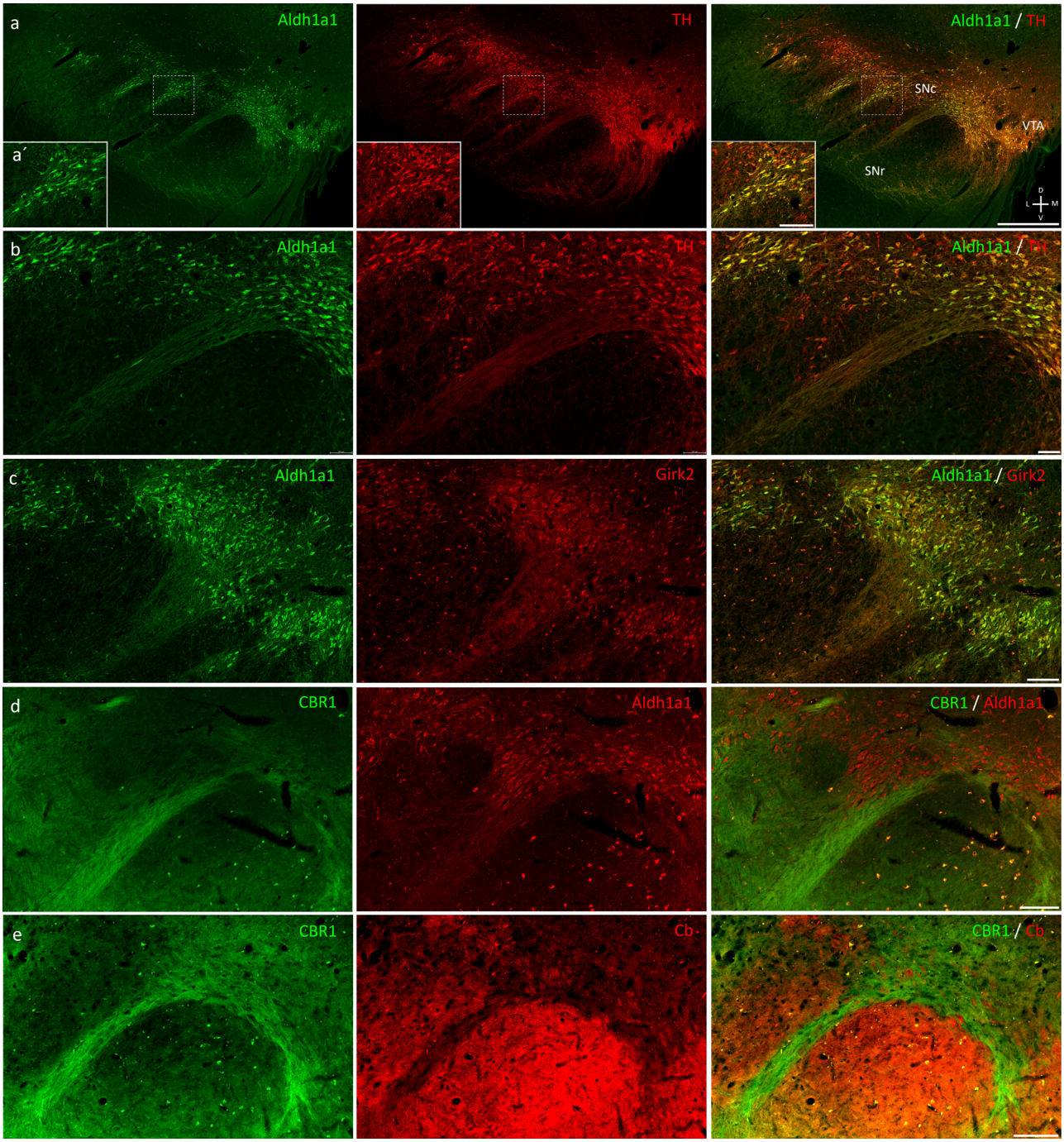

Fig. 5 | Dendritic processes with long trajectories extend dorsoventrally in the SNr. a Representative low-power images of TH + /Aldh1a1+ clusters of SNc ventral neurons and resultant ventrally extended dendrites in the SNr of a control monkey. **a'** Note the presence of striking clusters of neurons in the SNc. **b** Higher power images of TH + /Aldh1a1+ dendrites extending into the SNr. **c** High-power images of Aldh1a1 + /Girk2+ dendrites extending into the SNr. **d** High-power Image of SNr CBR1-labelled dendrites extending dorsally into the adjacent sector of the SNc concurring with Aldh1a1+ ventrally extending dendrites. **e** High-power image showing the apparent dendron structures in the control monkey midbrain. Calbindin labels the fibers in the SNr and avoids the SNc and CBR1+ axons. For all low-power analogous images see Supplementary Fig. 10. Abbreviations: SNc: *Substantia nigra pars compacta*; SNr: *Substantia nigra pars reticulata*; VTA: Ventral Tegmental Area; D: dorsal; V: ventral; M: medial; L: lateral. Scale bar: 1 mm (insets 250 μm).

precisely defined dopaminergic cluster subtypes. Integrating connectivity studies, a more precise characterization of Aldh1a1+ or Girk2+ dopaminergic neuron subpopulations, and thorough circuit investigations could play a key role in uncovering the mechanisms supporting neuronal vulnerability in Parkinson´s disease. This could, in turn, guide development of new therapeutic approaches, including subtype-specific pharmacological interventions.

Methods

Experimental animals

Thirteen adult naive male *Macaca fascicularis* NHPs were used in this study (R.C. Hartelust BV, Tilburg, The Netherlands). The monkeys were housed in the animal vivarium under standard conditions and handled in full keeping with European and Spanish animal care regulations (2010/63/UE and RD53/2013, respectively). The experimental protocols were approved

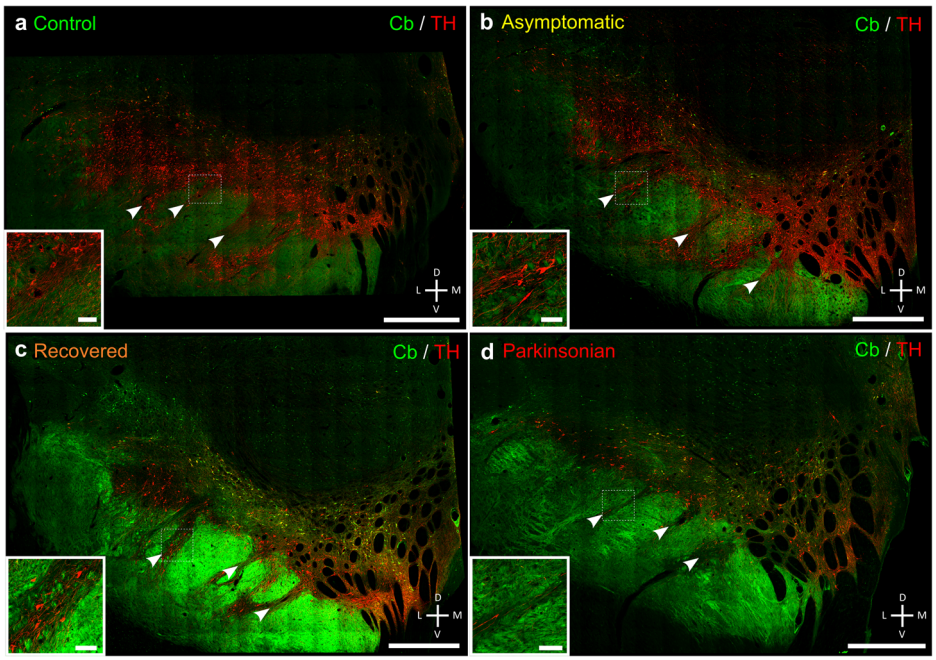

Fig. 6 | Loss of TH+ neurons and their dendrites located in the vSNc in parkinsonian monkeys. Representative confocal images of midbrain coronal sections at the level of the third cranial nerve immunostained for Cb and TH in Control **a**, Asymptomatic **b**, Recovered **c**, and Parkinsonian **d** monkeys. White arrows and insets show representative ventral dendrites. The greatest reduction of ventral dendrites occurs in monkeys with net and stable parkinsonism. D: dorsal; V: ventral; M: medial; L: lateral. Scale bar: 1 mm (inset **a**: 100 µm; inset **b**: 100 µm; inset **c**: 200 µm; inset **d**: 200 µm).

by the Ethical Committee for Research of the Fundación de Investigación HM Hospitales (CEEA-01/2015; CEEA-06/2015) as well as by the department of Animal Welfare of the Government of Madrid (PROEX 269/2015; PROEX 040/2016).

Two monkeys were used as controls (*Control* group) and received systemic administration *(i.v.)* of saline (NaCl 0.9%, vehicle of MPTP solution) every 2 weeks, whereas six monkeys were treated with MPTP (Sigma, Saint Louis, MO, USA) by systemic intravenous administration. under light anesthesia (ketamine 10 mg/kg; *i.m.)* using a dose regimen of 0.5 mg/kg every 2 weeks to obtain partial and slowly-progressive degeneration of the nigrostriatal dopaminergic system as described previously[24,25,93–95]. Motor status was assessed with a clinical-rating validated scale[96]. As each monkey has a different susceptibility to MPTP[97], the number of injections varied depending on the response to the toxin (*i.e.* individual sensitivity) until the motor score was reached. Two monkeys appeared to be more susceptible and displayed an evident and persistent parkinsonian syndrome after the first MPTP injection and therefore did not receive any further injection; these two monkeys form the *Parkinsonian* group. Two monkeys required two injections of MPTP to exhibit a clear motor phenotype, however they later showed substantial recovery and remained minimally affected (*Recovered* group)[24,98]. The *Asymptomatic* group was composed of two monkeys that did not show any motor phenotype even after three MPTP injections. All monkey records are shown in Supplementary Table 1. Throughout the duration of the study, none of the monkeys received dopaminergic medication. Analysis was performed on all MPTP-treated monkeys, both grouped together ($n = 6$) and per group ($n = 2$/group).

The retrograde neuroanatomical tracer unconjugated CTB (List Biological Laboratories, Campbell, CA) was pressure-delivered into the caudate nucleus of one hemisphere and the putamen of the contralateral hemisphere in four monkeys (bilateral injections); whereas in one additional monkey, CTB was delivered into the GPi of one hemisphere and into the GPe of the contralateral hemisphere.

Surgical anesthesia was induced by intramuscular injection of ketamine (5 mg/kg) and midazolam (0.5 mg/kg). Local anesthesia was implemented just before surgery with a 10% solution of lidocaine. Analgesia was achieved with a single intramuscular injection of flunixin meglumine (Finadyne®, 5 mg/kg) delivered at the end of the surgical procedure and repeated 24 and 48 h post-surgery. A similar schedule was followed for antibiotic coverage (ampicillin, 0.5 ml/day). After surgery, monkeys were kept under constant monitoring in individual cages with *ad libitum* access to food and water. Once they showed complete post-surgical recovery (24 h), they were returned to the animal vivarium and housed in groups for a follow-up of two weeks until final sacrifice.

Stereotaxic coordinates for the caudate and putamen were calculated from the atlas of Szabo and Cowan[99]. Coordinates for the caudate nucleus were 20 mm rostral to the interaural plane, 12 mm ventral to the cortical surface, and 5 mm lateral to the midline. Coordinates for the pre-commissural putamen were 20 mm rostral to the interaural plane, 16 mm ventral to the cortical surface and 19 mm lateral from the midline, whereas post-commissural putaminal injections were performed 13 mm rostral to the interaural plane, 15 mm ventral to the cortical surface and 12 mm lateral to the midline. Stereotaxic coordinates for GPe and GPi were calculated from the atlas of Lanciego and Vazquez[100]. Coordinates for the GPi were 4 mm caudal to the anterior commissure (ac), 1 mm ventral to the ac-posterior commissure (ac-pc) plane and 13 mm lateral to the midline; coordinates for the GPe were 4 mm caudal to ac, 1.5 mm dorsal to ac-pc plane and 14 mm lateral to the midline (Supplementary Fig. 11f, g). CTB deliveries were performed through a Hamilton® microsyringe in pulses of 0.1–1 µl/2 min for a total volume of 100 nl–5 µl/injection (5 mg/ml in 0.01 M PB, pH 7.5). Once completed, the needle was left in place for 15 min before withdrawal to minimize CTB reflux through the injection tract.

Necropsy and histological processing

Monkeys were deeply anesthetized with a terminal dose of sodium pentobarbital (200 mg/kg, i.p.) and perfused through the ascending aorta with an infusion pump. The perfusates consisted of a saline solution, followed by 4% paraformaldehyde in phosphate buffer and an ascending series of buffered sucrose solutions (5–10–20%). The brains were blocked in the coronal stereotaxic plane (plane 0 corresponding to the interaural plane) and sectioned (40 µm-thick sections) on a freezing microtome.

For detection of the different dopaminergic neuron subpopulations, combinations of double-labeling experiments were performed. Free-floating coronal sections were washed in tris-buffer and treated with citrate buffer (pH 6) for 30 min at 37 °C for antigen retrieval. Normal serum

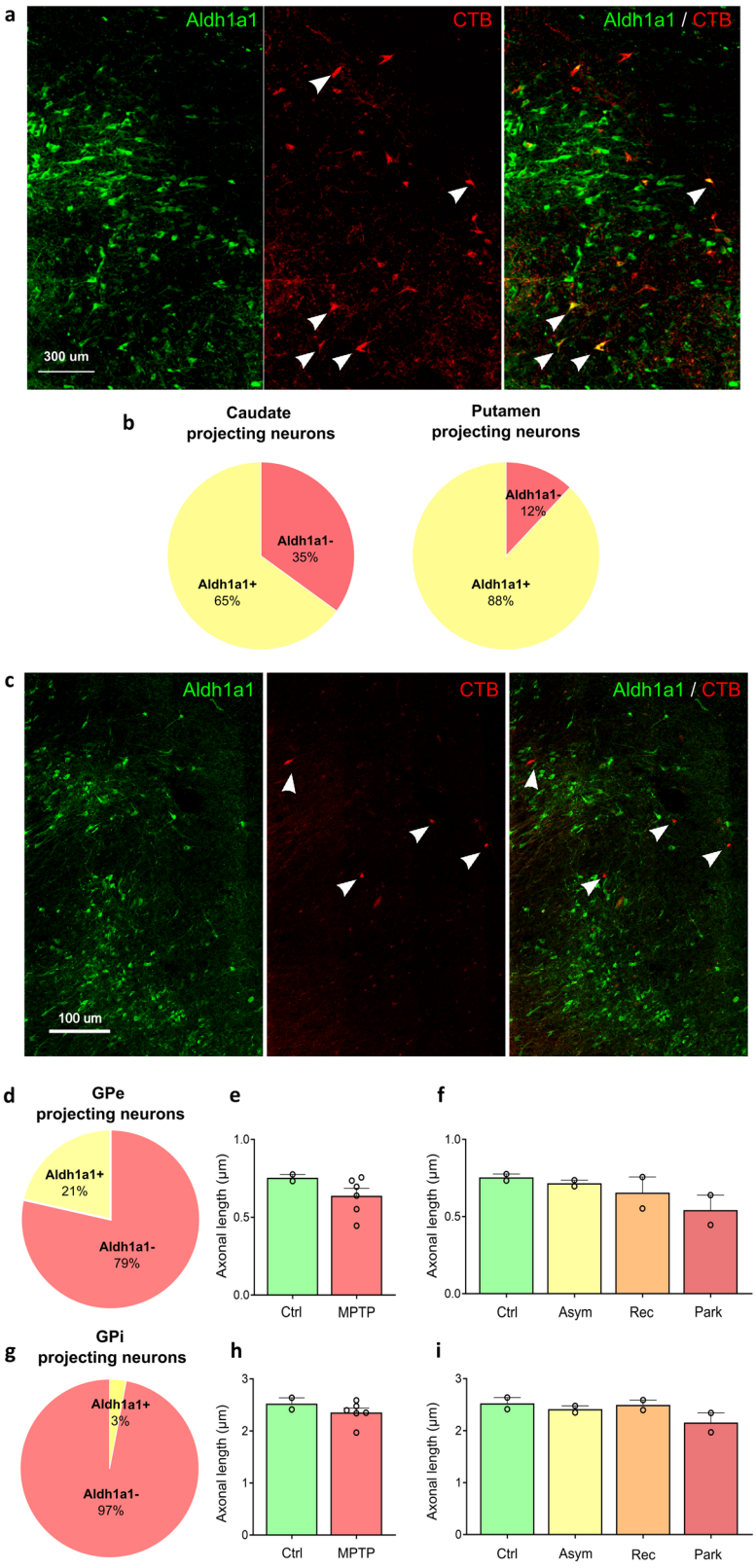

Fig. 7 | Aldh1a1+ neurons define the nigrostriatal dopaminergic projection. a Representative confocal images showing the expression of cholera toxin subunit B (CTB)-labeled midbrain neurons co-expressing Aldh1a1 after striatal tracer injection. White arrows show abundant Aldh1a1 + /CTB+ neurons. **b** Percentages of expression of Aldh1a1 + / CTB+ neurons in the monkey's midbrain with injections in the caudate ($n = 2$; 78 neurons) and putamen respectively ($n = 3$; 623 neurons). **c** Representative confocal images showing the expression of CTB-labeled midbrain neurons expressing Aldh1a1 after globus pallidus injection. White arrows show abundant Aldh1a1-/CTB+ neurons. **d** Percentages of expression of Aldh1a1 + / CTB+ neurons in the monkey's midbrain with injection in the external division if the globus pallidus (GPe) ($n = 1$; 127 neurons). **e**, **f** Quantification of TH-immunoreactive axonal length in the GPe in control and MPTP-treated monkeys ($n = 2$/group; MPTP $n = 6$). **g** Percentages of expression of Aldh1a1 + /CTB+ neurons in the monkey's midbrain with injection in the internal division if the globus pallidus (GPi) ($n = 1$; 139 neurons). **h**, **i** Quantification of TH-immunoreactive axonal length in the GPi in control and MPTP-treated monkeys ($n = 2$/group; MPTP $n = 6$). Data represent mean + SEM. Ctrl, control; Asym, asymptomatic; Rec, recovered; Park, parkinsonian.

was applied for 3 h to block non-specific binding sites. The sections were incubated at 4 °C for 72 h with primary antibodies directed against TH, Cb, Girk2, Alhd1a1, CBR1, and CTB. The sections were washed in tris-buffered solution and transferred for 2 h to a solution containing the corresponding secondary fluorescence antibodies.

For optical density quantification in the striatum and stereological counting in the GPe and GPi, free-floating immunohistochemistry was performed using a primary monoclonal anti-TH mouse antibody and a secondary biotinylated polyclonal anti-mouse antibody. Development of the immunoreaction was done using diaminobenzidine as substrate.

Table 1 | List of antibodies

Antibodies	Dilution	Source	Identifier	RRID
Primary antibodies				
Mouse anti Tyrosine Hydroxylase	1:1,000	Millipore	MAB5280	AB_2201526
Rabbit anti Tyrosine Hydroxylase	1:1,000	Sigma	AB152	AB_390204
Mouse anti Calbindin	1:7,000	Swant	CB300	AB_10000347
Rabbit anti Calbindin	1:10,000	Swant	CB38	AB_10000340
Rabbit anti G-protein-activated inward rectifying potassium type 2	1:400	Alomone Labs	APC-006	AB_2040115
Mouse anti Aldehyde Dehydrogenase 1_Family Member A1	1:200	Thermo Fisher	MA5-15692	AB_11009627
Mouse anti Cannabinoid receptor type 1	1:500	Synaptic Systems	258 008	AB_2864784
Rabbit anti Cholera Toxin Subunit B	1:1,000	Sigma	C3062	AB_258833
Secondary antibodies				
Goat anti-mouse Alexa Fluor 488	1:500	Thermo Fisher	A-11029	AB_2534072
Goat anti-rabbit Alexa Fluor 568	1:500	Thermo Fisher	A-11011	AB_143157
Horse anti-mouse, biotinylated	1:400	Vector Laboratories	BA-2000	AB_2313581

The sections were then dehydrated through graded ascending ethanol solutions, cleared in xylene, and cover slipped with DPX. All sections were processed simultaneously in all monkeys. For control purposes, all immunohistochemical stains included sections incubated without the corresponding primary antibody.

A complete list of antibodies, together with incubation concentrations and commercial sources is provided in Table 1.

Assessment of terminal densities in the striatum

The relative optical densities of TH+ fibers in the caudate nucleus, putamen, and ventral striatum were quantified in the diaminobenzidine developed sections using computer-assisted image analysis techniques (ImageJ 1.41o, National Institutes of Health, USA). Images were captured in black and white 8-bit monochrome using a digital camera (AxioCam HRc, Zeiss, Germany) attached to a Nikon *Multiphot* microphotography system. Digital images were captured under the same exposure settings for all experimental cases. Seven rostrocaudal sections, equally spaced at intervals of 2400 µm, were examined for each monkey. Three sections were more rostral, and four sections were more caudal to the midline decussation of the anterior commissure. The optical density of a 0.080 μm^2 region of white matter in the corpus callosum in the same section was subtracted as background. To quantify the dorsoventral dopaminergic gradient of the striatum, both the caudate and putamen were delineated into three equivalent dorsal, intermediate, and ventral subdivisions.

Midbrain sections sampled and neuronal quantification

Five to seven coronal sections, regularly spaced 1200 µm apart, covering the whole rostrocaudal extent of the midbrain were scanned under the microscope. Immunofluorescence sections were inspected using a Leica SPI TCS SP5 confocal laser-scanning microscope. To ensure appropriate visualization of the labeled elements and to avoid false positive results, the emission from the argon laser at 488 nm was filtered through a band pass filter of 505–530 nm and color-coded in green. The emission following excitation with the helium laser at 543 nm was filtered through a band pass filter of 560–615 nm and color-coded in red. Due to the large size of the region of interest, automated images were taken to obtain a mosaic of each midbrain with a 40× objective, where each quadrant was acquired in 5 sections in the z-axis with a resolution of 512 × 512 ppi. Co-localization and quantification were analyzed by blinded researchers for each marker using *ImageJ* (2.1.0/1.53c) software in 5 to 7 sections.

To investigate the expression of Girk2 and Aldh1a1 in the different catecholaminergic populations (TH +), sections were selected based on Sanchez-Gonzalez et al. [101], including the olfactory bulb and the *locus coeruleus*.

Stereological quantification of TH axons in the globus pallidus

The density of axons immunoreactive for TH was estimated in the GPe and GPi by means of the optical fractionator method by a blinded researcher using 3D hemispherical probes (*StereoInvestigator*® software, MicroBrightField, USA) as previously described[95,102]. Three TH immunostained coronal sections regularly spaced 2,400 µm apart were studied in each monkey. Virtual hemispheres (radius = 10 µm) were projected along the Z-axis, spaced in a sampling grid of 250 × 250 µm. A guard-zone 2 µm high was used on the top of the section. These parameters were set to reach an error coefficient below 0.10 (Gundersen, m = 0) and 0.05 (Gundersen, m = 1). The intersections of TH axons with the boundaries of the hemispheres, observed with a 100× immersion objective, were quantified. Total axonal length was calculated. To correct for potential differences in brain sizes, the volume of each nucleus was calculated by the Cavalieri method[103]. Axonal length density was defined as the total axonal length per volume of each nucleus[104].

Statistics and figures

Statistics were performed between data from the control group and the MPTP-treated groups using the *Statistica* 12 software (StatSoft Inc., Dell Software). Data normality was checked with the Kolmogorov–Smirnov test. Differences of neuronal numbers and axonal length density among groups were analyzed by one-way repeated measure analysis of variance (ANOVA) followed by the Bonferroni *post-hoc* test. When comparing the means of the control group with the MPTP-treated group, a two-sample non-parametric unpaired *t*-test (Mann-Whitney U test) was performed. All data are expressed as the mean ± standard error of the mean (SEM). The significance threshold was $P < 0.05$. Graphs were made with *GraphPad Prism* 6.01 for Windows (GraphPad® Software).

Images for figures were acquired on a Leica MICA microscope at 20× (high-power) and 63× (insets) magnification. Figures were made with *Inkscape* 1.1.

Data availability

All data needed to evaluate the conclusions are available in the main text or the Supplementary Material. Further information and request for resources and reagents should be directed to and will be provided by the corresponding authors.

Received: 17 April 2024; Accepted: 5 August 2024;
Published online: 02 September 2024

References

1. Blesa, J., Foffani, G., Dehay, B., Bezard, E. & Obeso, J. A. Motor and non-motor circuit disturbances in early Parkinson disease: which happens first? *Nat Rev. Neurosci*. **23**, 115–128 (2022).
2. Pineda-Pardo, J. D. S. A., Sánchez-Ferro, Á., Monje, M. H. G., Pavese, N. & Obeso, J. A. Onset pattern of nigrostriatal denervation in early Parkinson's disease. *Brain* **145**, 1018–1028 (2022).
3. Monje, M. H. G. et al. Motor Onset Topography and Progression in Parkinson's Disease: the Upper Limb Is First. *Movement Disorders* **36**, 905–915 (2021).
4. Damier, P., Hirsch, E. C., Agid, Y. & Graybiel, A. M. The substantia nigra of the human brain. II. Patterns of loss of dopamine-containing neurons in Parkinson's disease. *Brain* **122**, 1437–1448 (1999).
5. German, D. C., Manaye, K., Smith, W. K., Woodward, D. J. & Saper, C. B. Midbrain dopaminergic cell loss in parkinson's disease: Computer visualization. *Ann Neurol*. **26**, 507–514 (1989).
6. Brodsky, M. et al. Nigrosome 1 absence in de novo Parkinson disease. *Neurology* **90**, 522–523 (2018).
7. Hirsch, E. C. Biochemistry of Parkinson's disease with special reference to the dopaminergic systems. *Mol Neurobiol*. **9**, 135–142 (1994).
8. Giguère, N., Burke Nanni, S. & Trudeau, L.-E. On Cell Loss and Selective Vulnerability of Neuronal Populations in Parkinson's Disease. *Front Neurol*. **9**, 455 (2018).
9. Dauer, W. & Przedborski, S. Parkinson's disease: mechanisms and models. *Neuron* **39**, 889–909 (2003).
10. Surmeier, D. J., Obeso, J. A. & Halliday, G. M. Selective neuronal vulnerability in Parkinson disease. *Nat Rev Neurosci* **18**, 101–113 (2017).
11. Gaertner, Z., Azcorra, M., Dombeck, D. A. & Awatramani, R. Molecular heterogeneity in the substantia nigra: A roadmap for understanding PD motor pathophysiology. *Neurobiol Dis* **175**, 105925 (2022).
12. Poulin, J.-F., Gaertner, Z., Moreno-Ramos, O. A. & Awatramani, R. Classification of Midbrain Dopamine Neurons Using Single-Cell Gene Expression Profiling Approaches. *Trends Neurosci*. **43**, 155–169 (2020).
13. Garritsen, O., van Battum, E. Y., Grossouw, L. M. & Pasterkamp, R. J. Development, wiring and function of dopamine neuron subtypes. *Nat Rev. Neurosci*. **24**, 134–152 (2023).
14. Sjöstedt, E. et al. An atlas of the protein-coding genes in the human, pig, and mouse brain. *Science (1979)* **367**, eaay5947 (2020).
15. La Manno, G. et al. Molecular Diversity of Midbrain Development in Mouse, Human, and Stem. *Cells. Cell* **167**, 566–580.e19 (2016).
16. Blesa, J., Trigo-Damas, I., del Rey, N. L. G. & Obeso, J. A. The use of nonhuman primate models to understand processes in Parkinson's disease. *J Neural Transm (Vienna)* **125**, 1–11 (2018).
17. Kamath, T. et al. Single-cell genomic profiling of human dopamine neurons identifies a population that selectively degenerates in Parkinson's disease. *Nat Neurosci*. **25**, 588–595 (2022).
18. Tang, L. et al. A primate nigrostriatal atlas of neuronal vulnerability and resilience in a model of Parkinson's disease. *Nat Commun*. **14**, (2023).
19. Wang, Q. et al. Molecular profiling of human substantia nigra identifies diverse neuron types associated with vulnerability in Parkinson's disease. *Sci. Adv*. **10**, eadi8287 (2024).
20. Martirosyan, A. et al. Unravelling cell type-specific responses to Parkinson's Disease at single cell resolution. *Mol Neurodegener* **19**, 7 (2024).
21. Kamath, T. & Macosko, E. Z. Insights into Neurodegeneration in Parkinson's Disease from Single-Cell and Spatial Genomics. *Movement Disorders* **38**, 518–525 (2023).
22. Salmani, B. Y. et al. Transcriptomic atlas of midbrain dopamine neurons uncovers differential vulnerability in a Parkinsonism lesion model. *Elife* **12**, (2023).
23. Blesa, J. & Przedborski, S. Parkinson's Disease: animal models and dopaminergic cell vulnerability. *Front Neuroanat*. **8**, 155 (2014).
24. Blesa, J. et al. The nigrostriatal system in the presymptomatic and symptomatic stages in the MPTP monkey model: A PET, histological and biochemical study. *Neurobiol. Dis*. **48**, 79–91 (2012).
25. Blesa, J. et al. Progression of dopaminergic depletion in a model of MPTP-induced Parkinsonism in non-human primates. An 18F-DOPA and 11C-DTBZ PET study. *Neurobiol Dis*. **38**, 456–463 (2010).
26. Damier, P., Hirsch, E. C., Agid, Y. & Graybiel, A. M. The substantia nigra of the human brain. I. Nigrosomes and the nigral matrix, a compartmental organization based on calbindin D(28 K) immunohistochemistry. *Brain* **122**, 1421–1436 (1999).
27. Gerfen, C. R., Herkenham, M. & Thibault, J. The neostriatal mosaic: II. Patch- and matrix-directed mesostriatal dopaminergic and non-dopaminergic systems. *J Neurosci*. **7**, 3915–3934 (1987).
28. Lynd-Balta, E. & Haber, S. N. The organization of midbrain projections to the ventral striatum in the primate. *Neuroscience* **59**, 609–623 (1994).
29. Haber, S. N., Ryoo, H., Cox, C. & Lu, W. Subsets of midbrain dopaminergic neurons in monkeys are distinguished by different levels of mRNA for the dopamine transporter: comparison with the mRNA for the D2 receptor, tyrosine hydroxylase and calbindin immunoreactivity. *J Comp. Neurol*. **362**, 400–410 (1995).
30. Iravani, M. M. et al. A modified MPTP treatment regime produces reproducible partial nigrostriatal lesions in common marmosets. *Eur J Neurosci*. **21**, 841–854 (2005).
31. Fallon, J. H., Riley, J. N. & Moore, R. Y. Substantia nigra dopamine neurons: separate populations project to neostriatum and allocortex. *Neurosci. Lett*. **7**, 157–162 (1978).
32. Crittenden, J. R. et al. Striosome-dendron bouquets highlight a unique striatonigral circuit targeting dopamine-containing neurons. *Proc Natl Acad Sci USA* **113**, 11318–11323 (2016).
33. Pereira Luppi, M. et al. Sox6 expression distinguishes dorsally and ventrally biased dopamine neurons in the substantia nigra with distinctive properties and embryonic origins. *Cell Rep*. **37**, 109975 (2021).
34. Yamada, T., McGeer, P. L., Baimbridge, K. G. & McGeer, E. G. Relative sparing in Parkinson's disease of substantia nigra dopamine neurons containing calbindin-D28K. *Brain Res*. **526**, 303–307 (1990).
35. Lavoie, B. & Parent, A. Dopaminergic neurons expressing calbindin in normal and parkinsonian monkeys. *Neuroreport* **2**, 601–604 (1991).
36. Dopeso-Reyes, I. G. et al. Calbindin content and differential vulnerability of midbrain efferent dopaminergic neurons in macaques. *Front Neuroanat* **8**, 146 (2014).
37. Inoue, K. et al. Recruitment of calbindin into nigral dopamine neurons protects against MPTP-Induced parkinsonism. *Mov Disord* **34**, 200–209 (2019).
38. Blesa, J. & Vila, M. Parkinson disease, substantia nigra vulnerability, and calbindin expression: Enlightening the darkness? *Movement Disorders* **34**, 161–163 (2019).
39. Galter, D., Buervenich, S., Carmine, A., Anvret, M. & Olson, L. ALDH1 mRNA: Presence in human dopamine neurons and decreases in substantia nigra in Parkinson's disease and in the ventral tegmental area in schizophrenia. *Neurobiol Dis*. **14**, 637–647 (2003).
40. Liu, G. et al. Aldehyde dehydrogenase 1 defines and protects a nigrostriatal dopaminergic neuron subpopulation. *Journal of Clinical Investigation* **124**, 3032–3046 (2014).
41. Poulin, J. F. et al. Defining midbrain dopaminergic neuron diversity by single-cell gene expression profiling. *Cell Rep*. **9**, 930–943 (2014).

42. Wu, J. et al. Distinct Connectivity and Functionality of Aldehyde Dehydrogenase 1a1-Positive Nigrostriatal Dopaminergic Neurons in Motor Learning. *Cell Rep*. **28**, 1167–1181.e7 (2019).
43. Schein, J. C., Hunter, D. D. & Roffler-Tarlov, S. Girk2 expression in the ventral midbrain, cerebellum, and olfactory bulb and its relationship to the murine mutation weaver. *Dev. Biol*. **204**, 432–450 (1998).
44. Chung, C. Y. et al. Cell type-specific gene expression of midbrain dopaminergic neurons reveals molecules involved in their vulnerability and protection. *Hum Mol. Genet*. **14**, 1709–1725 (2005).
45. Mendez, I. et al. Cell type analysis of functional fetal dopamine cell suspension transplants in the striatum and substantia nigra of patients with Parkinson's disease. *Brain* **128**, 1498–1510 (2005).
46. Grealish, S. et al. The A9 dopamine neuron component in grafts of ventral mesencephalon is an important determinant for recovery of motor function in a rat model of Parkinson's disease. *Brain* **133**, 482–495 (2010).
47. Thompson, L., Barraud, P., Andersson, E., Kirik, D. & Björklund, A. Identification of dopaminergic neurons of nigral and ventral tegmental area subtypes in grafts of fetal ventral mesencephalon based on cell morphology, protein expression, and efferent projections. *J Neurosci*. **25**, 6467–6477 (2005).
48. Fudge, J. L. et al. Beyond the Classic VTA: Extended Amygdala Projections to DA-Striatal Paths in the Primate. *Neuropsychopharmacology* **42**, 1563–1576 (2017).
49. Reyes, S. et al. GIRK2 expression in dopamine neurons of the substantia nigra and ventral tegmental area. *J Comp Neurol*. **520**, 2591–2607 (2012).
50. Saunders, A. et al. Molecular Diversity and Specializations among the Cells of the Adult Mouse Brain. *Cell* **174**, 1015–1030.e16 (2018).
51. Azcorra, M. et al. Unique functional responses differentially map onto genetic subtypes of dopamine neurons. *Nat Neurosci* **26**, 1762–1774 (2023).
52. Dragicevic, E. et al. Cav1.3 channels control D2-autoreceptor responses via NCS-1 in substantia nigra dopamine neurons. *Brain* **137**, 2287–2302 (2014).
53. Duda, J., Pötschke, C. & Liss, B. Converging roles of ion channels, calcium, metabolic stress, and activity pattern of *Substantia nigra* dopaminergic neurons in health and Parkinson's disease. *J Neurochem* **139**, 156–178 (2016).
54. Masato, A., Plotegher, N., Boassa, D. & Bubacco, L. Impaired dopamine metabolism in Parkinson's disease pathogenesis. *Molecular Neurodegeneration 2019 14:1* **14**, 1–21 (2019).
55. Mathiharan, Y. K. et al. Structural insights into GIRK2 channel modulation by cholesterol and PIP 2. *Cell Rep*. **36**, 109619 (2021).
56. Chan, C. S. et al. 'Rejuvenation' protects neurons in mouse models of Parkinson's disease. *Nature* **447**, 1081–1086 (2007).
57. Li, H. et al. Generation of human A9 dopaminergic pacemakers from induced pluripotent stem cells. *Mol Psychiatry* **27**, 4407–4418 (2022).
58. McCaffery, P. & Drager, U. C. High levels of a retinoic acid-generating dehydrogenase in the meso-telencephalic dopamine system. *Proc Natl Acad Sci USA* **91**, 7772–7776 (1994).
59. Grimm, J., Mueller, A., Hefti, F. & Rosenthal, A. Molecular basis for catecholaminergic neuron diversity. *Proc Natl Acad Sci USA* **101**, 13891–13896 (2004).
60. Cossette, M., Levesque, M., Parent, A., Lévesque, M. & Parent, A. Extrastriatal dopaminergic innervation of human basal ganglia. *Neurosci. Res*. **34**, 51–54 (1999).
61. Prensa, L., Cossette, M. & Parent, A. Dopaminergic innervation of human basal ganglia. *J Chem Neuroanat* **20**, 207–213 (2000).
62. Smith, Y., Lavoie, B., Dumas, J. & Parent, A. Evidence for a distinct nigropallidal dopaminergic projection in the squirrel monkey. *Brain Res*. **482**, 381–386 (1989).
63. Haber, S. N. & Fudge, J. L. The primate substantia nigra and VTA: integrative circuitry and function. *Crit Rev Neurobiol* **11**, 323–342 (1997).
64. Parent, A., Lavoie, B., Smith, Y. & Bédard, P. The dopaminergic nigropallidal projection in primates: distinct cellular origin and relative sparing in MPTP-treated monkeys. *Adv. Neurol*. **53**, 111–116 (1990).
65. Gagnon, D. et al. Evidence for Sprouting of Dopamine and Serotonin Axons in the Pallidum of Parkinsonian Monkeys. *Front Neuroanat* **12**, 1–14 (2018).
66. Sgobio, C. et al. Aldehyde dehydrogenase 1-positive nigrostriatal dopaminergic fibers exhibit distinct projection pattern and dopamine release dynamics at mouse dorsal striatum. *Sci Rep* **7**, (2017).
67. Poulin, J.-F. et al. Mapping projections of molecularly defined dopamine neuron subtypes using intersectional genetic approaches. *Nat Neurosci*. **21**, 1260–1271 (2018).
68. del Rey, N. L. G. & García-Cabezas, M. Á. Cytology, architecture, development, and connections of the primate striatum: Hints for human pathology. *Neurobiol. Dis*. **176**, (2023).
69. Masato, A. et al. DOPAL initiates αSynuclein-dependent impaired proteostasis and degeneration of neuronal projections in Parkinson's disease. *NPJ Parkinsons Dis*. **9**, (2023).
70. Crittenden, J. R., Yoshida, T., Venu, S., Mahar, A. & Graybiel, A. M. Cannabinoid Receptor 1 Is Required for Neurodevelopment of Striosome-Dendron Bouquets. *eNeuro* **9**, (2022).
71. Davis, M. I. et al. The cannabinoid-1 receptor is abundantly expressed in striatal striosomes and striosome-dendron bouquets of the substantia nigra. *PLoS One* **13**, e0191436 (2018).
72. Evans, R. C. et al. Functional Dissection of Basal Ganglia Inhibitory Inputs onto Substantia Nigra Dopaminergic Neurons. *Cell Rep* **32**, 108156 (2020).
73. Golden, J. P. et al. Dopamine-Dependent Compensation Maintains Motor Behavior in Mice with Developmental Ablation of Dopaminergic Neurons. *Journal of Neuroscience* **33**, 17095–17107 (2013).
74. González-Rodríguez, P. et al. Disruption of mitochondrial complex I induces progressive parkinsonism. *Nature* **599**, 650–656 (2021).
75. Delignat-Lavaud, B. et al. Synaptotagmin-1-dependent phasic axonal dopamine release is dispensable for basic motor behaviors in mice. *Nat Commun* **14**, 4120 (2023).
76. Obeso, J. A., Rodriguez-Oroz, M. C., Lanciego, J. L., Diaz, M. R. & Rodriguez Diaz, M. How does Parkinson's disease begin? The role of compensatory mechanisms. *Trends Neurosci* **27**, 125–128 (2004).
77. Blesa, J. et al. Compensatory mechanisms in Parkinson's disease: Circuits adaptations and role in disease modification. *Exp Neurol* **298**, 148–161 (2017).
78. Evans, R. C. Dendritic involvement in inhibition and disinhibition of vulnerable dopaminergic neurons in healthy and pathological conditions. *Neurobiol Dis* **172**, (2022).
79. Zhai, S., Cui, Q., Simmons, D. N. V. & Surmeier, D. J. Distributed dopaminergic signaling in the basal ganglia and its relationship to motor disability in Parkinson's disease. *Curr Opin Neurobiol* **83**, 102798 (2023).
80. Bezard, E., Porras, C. G., Blesa, J. & Obeso, J. A. Compensatory mechanisms in experimental and human parkinsonism: potencial for new therapies. in *Handbook of Basal Ganglia Structure and Function: A Decade of Progress* (eds. Steiner, H. & Tseng, H. M.) (Elsevier, San Diego, 2009).

81. Covey, D. P., Mateo, Y., Sulzer, D., Cheer, J. F. & Lovinger, D. M. Endocannabinoid modulation of dopamine neurotransmission. *Neuropharmacology* **124**, 52 (2017).
82. Liu, Z. et al. Deficiency in endocannabinoid synthase DAGLB contributes to early onset Parkinsonism and murine nigral dopaminergic neuron dysfunction. *Nat Commun* **13**, (2022).
83. Mailleux, P. & Vanderhaeghen, J. J. Localization of cannabinoid receptor in the human developing and adult basal ganglia. Higher levels in the striatonigral neurons. *Neurosci Lett* **148**, 173–176 (1992).
84. Wallmichrath, I. & Szabo, B. Cannabinoids inhibit striatonigral GABAergic neurotransmission in the mouse. *Neuroscience* **113**, 671–682 (2002).
85. Szabo, B., Wallmichrath, I., Mathonia, P. & Pfreundtner, C. Cannabinoids inhibit excitatory neurotransmission in the substantia nigra pars reticulata. *Neuroscience* **97**, 89–97 (2000).
86. Henny, P. et al. Structural correlates of heterogeneous in vivo activity of midbrain dopaminergic neurons. *Nat. Neurosci.* **15**, 613 (2012).
87. Mena-Segovia, J., Winn, P. & Bolam, J. P. Cholinergic modulation of midbrain dopaminergic systems. *Brain Res. Rev.* **58**, 265–271 (2008).
88. Rodriguez, M. C., Obeso, J. A. & Olanow, C. W. Subthalamic nucleus-mediated excitotoxicity in Parkinson's disease: a target for neuroprotection. *Ann. Neurol.* **44**, S175–S188 (1998).
89. Pacelli, C. et al. Elevated mitochondrial bioenergetics and axonal arborization size are key contributors to the vulnerability of dopamine neurons. *Curr. Biol.* **25**, 2349–2360 (2015).
90. Carmichael, K. et al. Function and Regulation of ALDH1A1-Positive Nigrostriatal Dopaminergic Neurons in Motor Control and Parkinson's Disease. *Front Neural Circuits* **15**, (2021).
91. Graybiel, A. M. & Matsushima, A. Striosomes and matrisomes: Scaffolds for dynamic coupling of Volition and Action. *Annu. Rev. Neurosci.* **46**, (2023).
92. Janssen, P. et al. Visualizing advances in the future of primate neuroscience research. *Curr. Res. Neurobiol.* **4**, (2022).
93. Blesa, J. et al. Inter-hemispheric asymmetry of nigrostriatal dopaminergic lesion: a possible compensatory mechanism in Parkinson's disease. *Front Syst. Neurosci.* **5**, 92 (2011).
94. Rey, N. L.-G. del, Trigo-Damas, I., Obeso, J. A., Cavada, C. & Blesa, J. Neuron types in the primate striatum: stereological analysis of projection neurons and interneurons in control and parkinsonian monkeys. *Neuropathol. Appl. Neurobiol.* https://doi.org/10.1111/NAN.12812 (2022).
95. Jiménez-Sánchez, L. et al. Serotonergic innervation of the striatum in a nonhuman primate model of Parkinson's disease. *Neuropharmacology* **170**, (2020).
96. Kurlan, R., Kim, M. H. H. & Gash, D. M. M. The time course and magnitude of spontaneous recovery of parkinsonism produced by intracarotid administration of 1-methyl-4-phenyl-1,2,3,6-tetrahydropyridine to monkeys. *Ann. Neurol.* **29**, 677–679 (1991).
97. Potts, L. F. et al. Modeling Parkinson's disease in monkeys for translational studies, a critical analysis. *Exp. Neurol.* **0**, 133 (2014).
98. Mounayar, S. et al. A new model to study compensatory mechanisms in MPTP-treated monkeys exhibiting recovery. *Brain* **130**, 2898–2914 (2007).
99. Szabo, J. & Cowan, W. M. A stereotaxic atlas of the brain of the cynomolgus monkey (Macaca fascicularis). *J. Comparat. Neurol.* **222**, 265–300 (1984).
100. Lanciego, J. L. & Vázquez, A. The basal ganglia and thalamus of the long-tailed macaque in stereotaxic coordinates. A template atlas based on coronal, sagittal and horizontal brain sections. *Brain Struct. Funct.* **217**, 613–666 (2012).
101. Sánchez-González, M. A. et al. The primate thalamus is a key target for brain dopamine. *J. Neurosci.* **25**, 6076–6083 (2005).
102. Monje, M. H. G., Blesa, J., García-Cabezas, M. Á., Obeso, J. A. & Cavada, C. Changes in thalamic dopamine innervation in a progressive Parkinson's disease model in monkeys. *Mov. Disorders* **35**, 419–430 (2020).
103. Gundersen, H. J. G. G. & Jensen, E. B. The efficiency of systematic sampling in stereology and its prediction. *J. Microsc.* **147**, 229–263 (1987).
104. West, M. J. Space balls revisited: stereological estimates of length with virtual isotropic surface probes. *Front Neuroanat.* **12**, 1–6 (2018).
105. Paxinos, G., Huang, X.-F. & Toga, A. The Rhesus Monkey Brain in Stereotaxic Coordinates. *Faculty of Health and Behavioural Sciences - Papers (Archive)* (2000).

Acknowledgements

N.L.G.R was funded by grant S2017/BMD-3700 (NEUROMETAB-CM) from Comunidad de Madrid; N.H.P by Ayudantes de Investigacion from Comunidad de Madrid; N.E.G by Instituto de Salud Carlos III PFIS (FI21/000919); C.C by Chair in Neuroscience UAM-Fundacion Tatiana Pérez de Guzmán el Bueno; J.A.O by Ministerio de Ciencia e Innovación y Universidades (PID2019–111045RB-I00); and J.B. by Instituto de Salud Carlos III Miguel Servet Program (CP19/00200) and FIS (PI23/00672). Expert technical assistance was kindly provided by Raquel Márquez, Maria Ciorraga, Noelia Mercado, Elvira Roda, and Adriana Honrubia. Tireless support ensuring the highest standards of animal welfare was provided by Cristina Gil, Jennifer Ribeiro, Juan Santos, Eduardo Alvarez, and Goiaz Ariznabarreta. Alberto J. Rico, PhD, assisted us during ventriculography-guided stereotaxic surgical deliveries of tracer. We also recognize expert support received from Lola Morales and Alejandro Nieto-Guerrero from the Confocal Microscopy Core Unit at Universidad Autonoma de Madrid. Assistance received from Lawrence Phillips, MD, for English language editing of this manuscript is gratefully acknowledged. Finally, we thank Dr. Rajeshwar Awatramani for helpful discussions and insightful comments on the manuscript.

Author contributions

Conceptualization, C.C., J.A.O., and J.B.; Methodology, N.L.G., N.H.P., M.C., M.dC., N.E.G., I.T.D., J.L., C.C., and J.B.; Investigation, C.C., J.A.O. and J.B.; Funding Acquisition, C.C., J.A.O., and J.B.; Resources, C.C., J.A.O., and J.B.; Supervision, C.C., J.A.O., and J.B. Writing – Original Draft, J.A.O. and J.B.; Writing – Review & Editing, N.L.G., N.H.P., M.C., M.dC., N.E.G., I.T.D., M.H.M., J.L., C.C., J.A.O. and J.B. Final manuscript was reviewed and approved by all co-authors.

Competing interests

The authors declare no conflicts of interest.

Additional information

Supplementary information The online version contains supplementary material available at https://doi.org/10.1038/s41531-024-00777-0.

Correspondence and requests for materials should be addressed to José A. Obeso or Javier Blesa.

[1]HM CINAC (Centro Integral de Neurociencias Abarca Campal), Hospital Universitario HM Puerta del Sur, HM Hospitales, Madrid, Spain. [2]Instituto de Investigación Sanitaria HM Hospitales, Madrid, Spain. [3]PhD Program in Neuroscience Autónoma de Madrid University-Cajal Institute, Madrid, Spain. [4]Northwestern University, Feinberg School of Medicine, Chicago, IL, USA. [5]Network Center for Biomedical Research on Neurodegenerative Diseases (CIBERNED), Instituto Carlos III, Madrid, Spain. [6]Facultad HM de Ciencias de la Salud de la Universidad Camilo José Cela, Madrid, Spain. [7]Parkinson's Disease and Movement Disorders Center, Northwestern University Feinberg School of Medicine, Chicago, IL, USA. [8]CNS Gene Therapy Program, Center for Applied Medical Research (CIMA), University of Navarra, Pamplona, Spain. [9]Department of Anatomy, Histology and Neuroscience, School of Medicine, Autónoma de Madrid University, Madrid, Spain. [10]These authors contributed equally: Nagore Hernández-Pinedo, Megan Carrillo. ✉e-mail: jobeso.hmcinac@hmhospitales.com; jblesa.hmcinac@hmhospitales.com